PNAS BRIEF REPORT | BIOPHYSICS AND COMPUTATIONAL BIOLOGY
MICROBIOLOGY OPEN ACCESS

Bacterial defense and phage counterdefense lead to coexistence in a modeled ecosystem

Ofer Kimchi[a], Yigal Meir[b,c], and Ned S. Wingreen[a,d,1]

Edited by Ralph Isberg, Tufts University School of Medicine, Boston, MA; received July 18, 2024; accepted September 29, 2024

Bacteria have evolved many defenses against invading viruses (phage). Despite the many bacterial defenses and phage counterdefenses, in most environments, bacteria and phage coexist, with neither driving the other to extinction. How is coexistence realized in the context of the bacteria/phage arms race, and how are immune repertoire sizes determined in conditions of coexistence? Here we develop a simple mathematical model to consider the evolutionary and ecological dynamics of competing bacteria and phage with different immune/counterimmune repertoires. We find an ecologically stable fixed point exhibiting coexistence, in agreement with the experimental observation that each individual bacterium typically carries multiple defense systems, though fewer than the maximum number possible. However, in simulations, the populations typically remain dynamic, exhibiting chaotic fluctuations around this fixed point. These dynamics enable coexistence even when phage (predator) strains outnumber bacteria (prey) strains. We obtain quantitative predictions for the mean, amplitude, and timescale of these dynamics. Our results provide a framework for understanding the evolutionary and ecological dynamics of the bacteria/phage arms race and demonstrate how bacteria/phage coexistence can stably arise from the coevolution of bacterial defense systems and phage counterdefense systems.

bacteria | phage | ecology | model | coexistence

Bacteria and the viruses that infect them (phage) have been engaged in an arms race spanning eons. Each bacterium typically carries many defense systems to protect against phage (1). Simultaneously, phage counterdefense systems enable them to evade these bacterial defenses (2). Both bacterial defense systems and phage counterdefense systems impose a fitness cost on the strains that carry them (3, 4). In bacteria, for example, both metabolic costs associated with protein production (5) as well as inadvertent self-targeting (6) contribute to the fitness cost. In the absence of selection pressure from the opposing species, these systems are therefore quickly lost, over the timescale of a few generations (7). We sought to understand the coevolution of these systems. What determines the size of a bacterial cell's immune repertoire and a single phage's counterimmunity repertoire?

The multiplicity of defense systems may enable bacteria to repel phage invaders by spreading defense systems through horizontal gene transfer (8). This 'pan-immunity hypothesis' explains boom and bust cycles of phage and bacteria as arising from subsequent rounds of phage invasion and bacterial defense. In contrast, we wanted to study how persistent coexistence of phage and bacteria is realized within the context of the defense/counterdefense arms race.

We consider a mixture of bacterial strains with population densities B_i and phage strains with densities P_j. Each bacterial strain carries a subset of a total number n^{tot} possible defense systems . Bacterial strains carrying more systems have a smaller growth rate α_i. Similarly, each phage strain carries a set of counterdefense systems, such that phage j can infect bacteria i if it has a corresponding counterdefense system for each of bacteria i's defense systems (9). The cost of counterdefense systems is imposed on the phage burst size $b_j + 1$. Bacterial and phage strain death rates are given by μ_i and δ_j, respectively. Finally, we include steady immigration fluxes λ_i and ν_j for the bacteria and phage. The system's dynamics are given by

$$\frac{dB_i}{dt} = B_i\left(\alpha_i - \mu_i - \sum_j k_{ij}P_j\right) + \lambda_i; \quad \frac{dP_j}{dt} = P_j\left(-\delta_j + b_j\sum_i k_{ij}B_i\right) + \nu_j, \quad [1]$$

where the infection rate $k_{ij} = k$ if phage j can infect bacteria i and 0 otherwise, and where we have neglected delays associated with phage reproduction (10). For simplicity, we focus on the case where each defense/counterdefense system has the same cost, and the immigration and death rates are strain-independent. We define a "largest positive-growth

Author affiliations: [a]Lewis-Sigler Institute for Integrative Genomics, Princeton University, Princeton, NJ 08544; [b]Department of Physics, Ben-Gurion University, Be'er Sheva 84105, Israel; [c]Department of Physics, Princeton University, Princeton, NJ 08544; and [d]Department of Molecular Biology, Princeton University, Princeton, NJ 08544

Author contributions: O.K., Y.M., and N.S.W. designed research; performed research; analyzed data; and wrote the paper.

The authors declare no competing interest.

[1]To whom correspondence may be addressed. Email: wingreen@princeton.edu.

This article contains supporting information online at https://www.pnas.org/lookup/suppl/doi:10.1073/pnas.2414229121/-/DCSupplemental.

Published October 25, 2024.

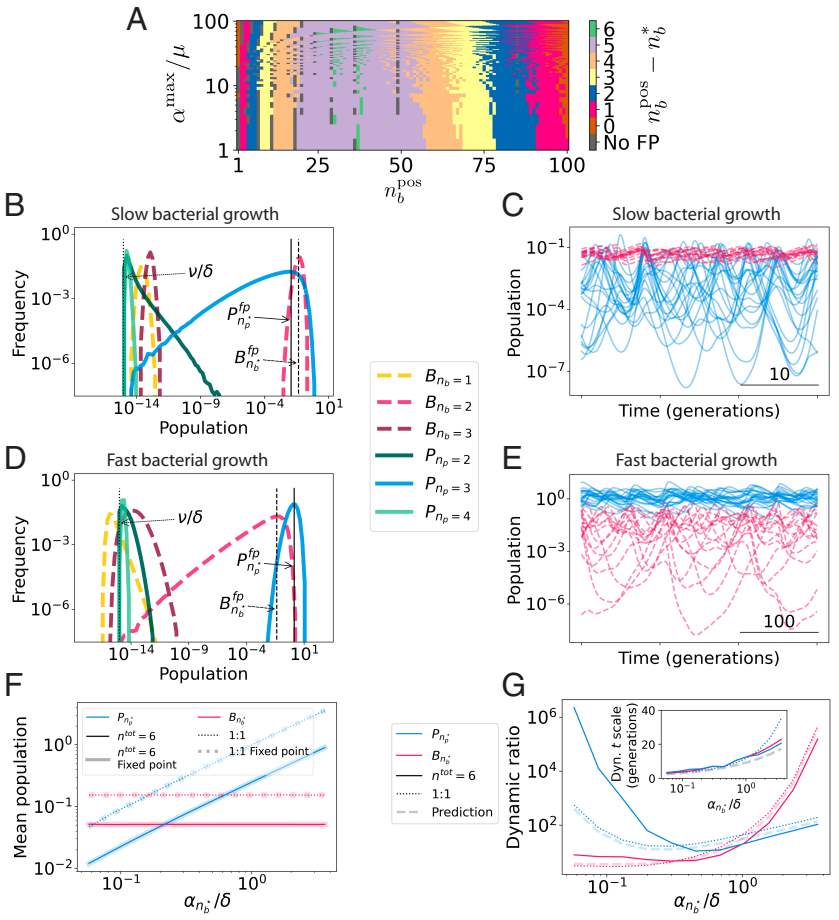

Fig. 1. Fixed-point and dynamical simulation results. (*A*) Predicted ecological fixed point for $n^{\text{tot}} = 110$ total defense systems, with $n_p^{\text{pos}} = 100$ maximum counterdefense systems per phage strain. Distance between predicted ecological fixed point $n_b^\star$ and maximal number of defense systems per bacterial strain, n_b^{pos}, is shown as a function of n_b^{pos} and the ratio between the growth rate of bacteria with no defense systems, $\alpha^{\max}$, and the death rate of bacteria, μ. Gray points represent parameters for which no ecologically stable fixed point is predicted. (*B*) Representative simulation results for an $n^{\text{tot}} = 6$ system with $\alpha^{\max}/\delta = 0.1$ and $\alpha_{n_b^\star}/\delta \approx 5.7 \times 10^{-2}$, displaying the histogram of population densities of bacterial and phage strains with different numbers of defense/counterdefense systems per strain. (*C*) Population dynamics of bacteria with $n_b = n_b^\star = 2$ defense systems each (red) and phage with $n_p = n_p^\star = 3$ counterdefense systems each (blue) in the $n^{\text{tot}} = 6$ simulation of panel (*B*). (*D* and *E*) Representative simulation results as in (*B* and *C*), but with bacterial growth rate increased to $\alpha^{\max}/\delta = 10$ (and $\alpha_{n_b^\star}/\delta \approx 5.7$). (*F*) Dependence of mean population densities for $n^{\text{tot}} = 6$ system (narrow solid curves), $n^{\text{tot}} = 0$ system (narrow dotted curves), and analytical dynamical fixed-point prediction from Eq. **1** (corresponding wide curves). (*G*) Dependence of dynamic ratio (main panel) and timescale of dynamics (*Inset*) for $n^{\text{tot}} = 6$ system (solid curves), $n^{\text{tot}} = 0$ system (dotted curves), and analytical prediction (*SI Appendix*, Eq. **S10**; dashed curves). Here, initial conditions were kept constant independent of *x*-axis parameter variation. The dynamic ratio measures the amplitude of fluctuations and is defined as the typical ratio of local maxima to local minima. See *SI Appendix*, sections S3 and S4 for further discussion.

repertoire size" for bacteria and phage, such that bacteria with $n_b > n_b^{\text{pos}}$ defense systems have a negative net growth rate $\alpha - \mu$, and phage with $n_p > n_p^{\text{pos}}$ counterdefense systems have a negative net burst size b.

We first address Eqs. **1** analytically. For a system composed exclusively of bacteria with n_b defense systems and phage with n_p counterdefense systems, a dynamically stable fixed point (dfp) can be found by solving $\frac{dB_i}{dt} = \frac{dP_j}{dt} = 0$. Due to symmetry, at this dfp , all bacterial strains with n_b defense systems are present at equal population densities $B_{n_b}^{\text{fp}}$, and all phage strains with n_p counterdefense systems are present at equal population densities $P_{n_p}^{\text{fp}}$. For certain combinations $(n_b^\star, n_p^\star)$, this dfp will also be an ecologically stable fixed point (efp) with respect to invasions by bacteria with $n_b^\star \pm 1$ defense systems, and to phage with $n_p^\star \pm 1$ counterdefense systems (*SI Appendix*, sections S1 and S2). At this efp, bacteria typically carry fewer than the maximal number of defense systems allowed by a positive growth rate, and similarly phages carry fewer than the maximal number of counterdefense systems (Fig. 1*A*).

We next turn to dynamical simulations. We consider a system with $n^{\text{tot}} = 6$ possible defense/counterdefense systems, with parameters such that $n_b^{\text{pos}} = 3$ and $n_p^{\text{pos}} = 4$, and for which we predict the existence of an efp with $(n_b^\star, n_p^\star) = (2, 3) < (n_b^{\text{pos}}, n_p^{\text{pos}})$ (*SI Appendix*, Eq. **S5**). At this efp, both bacterial growth rate and phage burst size are roughly half their maximum values. After a short transient period, we find that all populous bacterial strains have $n_b^\star$ defense systems, and all populous phage have $n_p^\star$ counterdefense systems (Fig. 1*B*). In the absence of immigration ($\lambda = \nu = 0$) only these strains survive. The analytically predicted dfp population densities predict well the time-averaged population densities of these strains (Fig. 1*B*, vertical lines). However, the system displays persistent chaotic dynamics (Fig. 1*C*; Lyapunov exponent = 0.08; see *SI Appendix*, section S3) (11).

These chaotic population fluctuations enable coexistence to be maintained even when the number of phage "predator" strains, $\binom{n^{\text{tot}}}{n_p^\star}$, exceeds the number of bacterial "prey" strains $\binom{n^{\text{tot}}}{n_b^\star}$ (12, 13). For different parameter choices, the chaotic fluctuations enabling this coexistence may either be largest in the phage population (as in Fig. 1 *B* and *C*) or largest in the bacterial population (as in Fig. 1 *D* and *E*). This variation in the dynamics comes with no apparent effect on the coexistence itself: we find that all bacteria with $n_b^\star$ defense systems and all phage with $n_p^\star$ counterdefense systems coexist in all cases we examined, even in the absence of immigration, $\lambda = \nu = 0$. Sufficient parameter heterogeneity can lead some strains to go extinct, but we found no extinction within 10^6 generations for moderate amounts of parameter heterogeneity ($\mathcal{O}(10^{-5})$).

While the average population densities are well predicted by the dfp population densities (Fig. 1*F*), the dynamics cannot be predicted by fixed-point analysis. Helpfully, we find a quantitatively similar parameter dependence of dynamics in the analytically tractable $n^{\text{tot}} = 0$ case, corresponding to a minimal oscillatory system of one bacterial strain and one phage strain ("1:1 case"; see *SI Appendix*, section S4). Both the

parameter-dependent dynamic ratio (i.e., the amplitude of fluctuations) and the dynamics' timescale are in quantitative agreement between the $n^{\text{tot}} = 6$ and 1:1 cases (Fig. 1*G*). Using the 1:1 system as a guide, we can thus predict the parameter-dependent features of the chaotic dynamics for more complex cases with multiple bacterial and phage strains.

Our model makes several simplifying assumptions. While we have considered all defense systems to be qualitatively interchangeable, defense systems in nature operate through different mechanisms and may have qualitatively different effects on both the growth cost to the bacterium and on the success or failure of the invading phage (and similarly for phage counterdefense systems) (3). Interactions among defense systems may also change their efficacies (14, 15). We have also focused exclusively on obligate lytic (virulent) phage, neglecting alternative phage infection strategies (16). Although temperate phage may qualitatively affect the behavior of many phage–bacteria interactions (17), here, the effect of superimmunity exclusion (i.e., that lysogens are immune to infection by phage of the same strain that lysogenized them) may be considered as a special case of a defense system. Similarly, chronic infections wherein phages reproduce and exit the cell without cell lysis may be considered as a modification of the infection rate k and the burst size b. Furthermore, although we have assumed well-mixed populations, spatial organization likely affects both the dynamics and coexistence of phage/bacteria communities, especially in nonaquatic environments (18). In this regard, abortive infection defenses will be a fruitful topic for future work. Finally, a variant of the model described by Eqs. **1** without immigration but allowing strains to stochastically gain, lose, and exchange systems with one another through mutations and horizontal gene transfer, yields qualitatively similar results (*SI Appendix*, section S3).

In summary, we have developed a model for the dynamics of competing phage and bacteria with different sets of defense and counterdefense systems. A fixed-point analysis (confirmed by dynamical simulations) indicates that phage and bacteria typically evolve to have more than one and fewer than the maximum number of defense/counterdefense systems in each strain. This qualitative behavior has been observed in nature and has previously been explained by the pan-immunity hypothesis, which argues that invading phage can be driven to extinction as long as some bacteria within a community are immune to the invading phage, and that this immunity can be conferred to other bacteria through horizontal gene transfer (8). In contrast, we find that within our model, large immunity and counterimmunity repertoires emerge naturally and enable bacteria/phage coexistence. This coexistence is manifested in persistent chaotic dynamics, with the mean, amplitude, and timescale of these dynamics well predicted by an analysis based on the competition between a single bacterial and a single phage strain. Although the ecological fixed point of the system $(n_b^\star, n_p^\star)$ depends on the details of defense and counterdefense system costs (*SI Appendix*, Eq. S5), we find that the qualitative dynamics depend only on the ratio α/δ (*SI Appendix*, Eqs. **S13** and **S18**). Thus, there are two main regimes of system behavior: compared to phage death rate, the bacterial growth rate may either be slow (Fig. 1 *B* and *C*) or fast (Fig. 1 *D* and *E*). Finally, although we have focused our analytical analysis on symmetric systems, our simulations demonstrate that even nonsymmetric systems with modest amounts of heterogeneity are not limited by the principle of competitive exclusion in our model. Thus, we find that the chaotic dynamics of the system enable the coexistence of more phage (predator) strains than bacterial (prey) strains, exceeding the biodiversity predicted by other frameworks such as "kill-the-winner" (19).

The discovery that bacteria typically carry multiple coexisting defense systems (and phage, multiple counterdefense systems) has raised many questions. Chief among these, what controls the number and type of defense and counterdefense systems in a particular bacterium or phage? One possibility is that these systems are controlled by happenstance, with horizontal gene transfer mediating random gains and losses of systems. Alternatively, our simple model suggests that states of evolutionary stability—albeit with fluctuations about these states—may provide a helpful guiding perspective.

Materials and Methods

Simulations were performed using Python version 3.9.13. Details of derivations and simulation methodology may be found in *SI Appendix*.

Data, Materials, and Software Availability. There are no data underlying this work.

ACKNOWLEDGMENTS. We thank Wenping Cui, Simon Levin, and Pankaj Mehta for useful discussions. This work was supported in part by Grant No. DAF2024-342781 from the Chan Zuckerberg Initiative DAF, an advised fund of Silicon Valley Community Foundation, and by the Peter B. Lewis '55 Lewis-Sigler Institute/Genomics Fund through the Lewis-Sigler Institute for Integrative Genomics at Princeton University (O.K.). This work was performed in part at Aspen Center for Physics, which is supported by NSF Grant PHY-1607611.

1. H. Georjon, A. Bernheim, The highly diverse antiphage defence systems of bacteria. *Nat. Rev. Microbiol.* **21**, 686–700 (2023).
2. K. Murtazalieva, A. Mu, A. Petrovskaya, R. D. Finn, The growing repertoire of phage anti-defence systems. *Trend. Microbiol.* 1–17 (2024).
3. H. G. Hampton, B. N. Watson, P. C. Fineran, The arms race between bacteria and their phage foes. *Nature* **577**, 327–336 (2020).
4. S. Srikant, C. K. Guegler, M. T. Laub, The evolution of a counter-defense mechanism in a virus constrains its host range. *eLife* **11**, 1–25 (2022).
5. P. F. Vale *et al.*, Costs of CRISPR-Cas-mediated resistance in *Streptococcus thermophilus*. *Proc. R. Soc. B: Biol. Sci.* **282**, 20151270 (2015).
6. M. Pleška *et al.*, Bacterial autoimmunity due to a restriction-modification system. *Curr. Biol.* **26**, 404–409 (2016).
7. J. M. Borin *et al.*, Rapid bacteria-phage coevolution drives the emergence of multiscale networks. *Science* **382**, 674–678 (2023).
8. A. Bernheim, R. Sorek, The pan-immune system of bacteria: Antiviral defence as a community resource. *Nat. Rev. Microbiol.* **18**, 113–119 (2020).
9. S. A. Levin, L. A. Segel, F. R. Adler, Diffuse coevolution in plant–herbivore communities. *Theor. Popul. Biol.* **37**, 171–191 (1990).
10. R. S. Eriksen, N. Mitarai, K. Sneppen, Sustainability of spatially distributed bacteria-phage systems. *Sci. Rep.* **10**, 3154 (2020).
11. E. H. Kerner, A statistical mechanics of interacting biological species. *Bull. Math. Biophys.* **19**, 121–146 (1957).
12. O. Kimchi, Y. Meir, N. S. Wingreen, Lytic and temperate phage naturally coexist in a dynamic population model. *ISME J.* **18**, 1–5 (2024).
13. J. Huisman, F. J. Weissing, Biodiversity of plankton by species oscillations and chaos. *Nature* **402**, 407–410 (1999).
14. C. F. Arias, F. J. Acosta, F. Bertocchini, M. A. Herrero, C. Fernández-Arias, The coordination of anti-phage immunity mechanisms in bacterial cells. *Nat. Commun.* **13**, 1–11 (2022).
15. Y. Wu *et al.*, Bacterial defense systems exhibit synergistic anti-phage activity. *Cell Host Microbe* **32**, 557–572.e6 (2024).
16. S. Mäntynen, E. Laanto, H. M. Oksanen, M. M. Poranen, S. L. Díaz-Muñoz, Black box of phage–bacterium interactions: Exploring alternative phage infection strategies. *Open Biol.* **11**, 8–10 (2021).
17. M. G. Cortes, Y. Lin, L. Zeng, G. Balázsi, From bench to keyboard and back again: A brief history of lambda phage modeling. *Annu. Rev. Biophys.* **50**, 117–134 (2021).
18. S. Testa *et al.*, Spatial structure affects phage efficacy in infecting dual-strain biofilms of *Pseudomonas aeruginosa*. *Commun. Biol.* **2**, 1–12 (2019).
19. T. F. Thingstad, Elements of a theory for the mechanisms controlling abundance, diversity, and biogeochemical role of lytic bacterial viruses in aquatic systems. *Limnol. Oceanogr.* **45**, 1320–1328 (2000).

Supplement: Bacterial defense and phage counter-defense lead to coexistence in a modeled ecosystem

S1 Deriving the conditions for an ecologically stable fixed point

To find the conditions defining an ecologically stable fixed point, we start from Eqs. 1, making the simplifications discussed in the main text, and assuming that the immigration terms λ and ν are negligible for the purpose of the following analyses. We consider a system composed exclusively of bacteria with n_b defense systems and phage with n_p counter-defense systems. At a dynamical fixed point of such a system, due to symmetry, all $\binom{n^{\text{tot}}}{n_b}$ bacterial strains with n_b defense systems are present at equal population densities $B^{\text{fp}}_{n_b}$, and all $\binom{n^{\text{tot}}}{n_p}$ phage strains with n_p counter-defense systems are present at equal population densities $P^{\text{fp}}_{n_p}$. This dynamical fixed point is given by

$$\begin{aligned} B^{\text{fp}}_{n_b} &= \frac{\delta}{k b_{n_p} \binom{n_p}{n_b}}, \\ P^{\text{fp}}_{n_p} &= \frac{\alpha_{n_b} - \mu}{k \binom{n^{\text{tot}} - n_b}{n_p - n_b}}, \end{aligned} \tag{S1}$$

where $\binom{n_p}{n_b}$ is the number of bacterial strains each phage strain can infect, and $\binom{n^{\text{tot}}-n_b}{n_p-n_b}$ is the number of phage strains that can infect each bacterial strain. α_{n_b} is the growth rate of bacteria with n_b defense systems, and is given by $\alpha_{n_b} = g(n_b)$ with a monotonically decreasing growth function g. Similarly, $b_{n_p} + 1$ is the burst size of phage carrying n_p counter-defense systems, and is given by $b_{n_p} + 1 = h(n_p)$ for a monotonically-decreasing function h. (Note that the effective burst size b takes into account the loss of the infecting phage particle). We assume g and h are concave functions, but our results largely hold if they are convex (except in the $n^{\text{tot}} \to \infty$ limit; see Supplementary Section S2).

This dynamical fixed point will further be an ecological fixed point if it is stable to invasions by bacteria with a different number of defense systems, or to phage with a different number of counter-defense systems. This will occur if the growth rates of such invading strains at the dynamical fixed point are negative. We refer to such an ecologically stable fixed point as $(n^\star_b, n^\star_p)$. The growth rate of an invading bacterial strain with $n^\dagger_b$ defense systems at the ecological fixed point would be

$$\frac{dB_{n^\dagger_b}}{dt} = B_{n^\dagger_b} \left(\alpha_{n^\dagger_b} - \mu - k \binom{n^{\text{tot}} - n^\dagger_b}{n^\star_p - n^\dagger_b} P^{\text{fp}}_{n^\star_p} \right), \tag{S2}$$

where $B_{n^\dagger_b}$ is the population of the invading bacterial strain. Similarly, the growth rate of an invading phage strain with $n^\dagger_p$ counter-defense systems would be

$$\frac{dP_{n^\dagger_p}}{dt} = P_{n^\dagger_p} \left(-\delta + k b_{n^\dagger_p} \binom{n^\dagger_p}{n^\star_b} B^{\text{fp}}_{n^\star_b} \right). \tag{S3}$$

These terms are negative for invading bacterial strains with $n^\dagger_b = n^\star_b \pm 1$ defense systems, and for invading phage strains with $n^\dagger_p = n^\star_p \pm 1$ counter-defense systems, when

$$
\begin{aligned}
\frac{\alpha_{n_b^\star+1}-\mu}{\alpha_{n_b^\star}-\mu} &< \frac{n_p^\star-n_b^\star}{n^{\text{tot}}-n_b^\star}, \\
\frac{\alpha_{n_b^\star}-\mu}{\alpha_{n_b^\star-1}-\mu} &> \frac{n_p^\star-n_b^\star+1}{n^{\text{tot}}-n_b^\star+1}, \\
\frac{b_{n_p^\star+1}}{b_{n_p^\star}} &< \frac{n_p^\star-n_b^\star+1}{n_p^\star+1}, \\
\frac{b_{n_p^\star}}{b_{n_p^\star-1}} &> \frac{n_p^\star-n_b^\star}{n_p^\star}.
\end{aligned}
\tag{S4}
$$

By taking the natural logarithm and substituting derivatives for differences, we arrive at the simplified expression

$$
\begin{aligned}
n_p^\star &= n^{\text{tot}}\left[1+\frac{d}{dn_b}\log\left(\frac{\alpha_{n_b}}{\mu}-1\right)\right]\Bigg|_{n_b=n_b^\star}, \\
n_b^\star &= -n_p^\star\left[\frac{d}{dn_p}\log\left(b_{n_p}\right)\right]\Bigg|_{n_p=n_p^\star}.
\end{aligned}
\tag{S5}
$$

S2 Ecological fixed point behavior as $n^{\text{tot}} \to \infty$

The behavior of the ecological fixed point defined by Eqs. (S5) as $n^{\text{tot}} \to \infty$ depends on how n_b^{pos} and n_p^{pos} scale with n^{tot}. Since ecological stability requires $n_p^\star > n_b^\star$, $n_p^{\text{pos}} > n_b^{\text{pos}}$ must hold to avoid the trivial outcome with no phage present. This inequality is biologically reasonable given the complexity required of defense systems compared to the relative simplicity of counter-defense systems; as an example, consider the immensely complex Type 1-F CRISPR-Cas system which can be evaded by phage that express a single short RNA molecule [S1]. As $n^{\text{tot}} \to \infty$, there are therefore three possibilities: 1) n_b^{pos} and n_p^{pos} are both intensive; 2) n_b^{pos} and n_p^{pos} are both extensive; 3) n_b^{pos} is intensive while n_p^{pos} is extensive. We find that in cases (1) and (2), $n_b^\star$ and $n_p^\star$ are approximately equal to n_b^{pos} and n_p^{pos}, respectively, as $n^{\text{tot}} \to \infty$. However, surprisingly, in case (3) and for concave cost functions g and h, $n_b^{\text{pos}} - n_b^\star$ and $n_p^{\text{pos}} - n_p^\star$ both grow with n^{tot}. In this case, each individual bacterium optimally carries a subset of possible defense systems, even though it could carry far more and still continue to grow (and similarly for phage).

S3 Details of dynamical simulations

We use the following parameters in our simulations, with time units such that $\delta = 1$ and population density units such that $k = 1$: $\mu = 10^{-2}$; $\lambda = \nu = 10^{-15}$; $b^{\max} = 15$. Bacterial growth rate α is varied as described in the main text; all other parameters are kept constant throughout. The bacterial death rate $\mu = 10^{-2}$ was chosen to be much smaller than the phage death rate δ so that we can explore the $\alpha < \delta$ regime while maintaining $\mu \ll \alpha$, such that bacterial populations are primarily limited by phage predation. For example, for $\alpha_{n_b^*} \approx 0.05$ as in Fig. 1b,c, the rate of bacterial death due to phage predation at the dynamical fixed point, $\binom{n^{\text{tot}}-n_b^\star}{n_p^\star-n_b^\star} k P_{n_p^\star}^{\text{fp}}$, is approximately $5\times$ larger than μ; for $\alpha_{n_b^*} \approx 5$ as in Fig. 1d,e, it is approximately $500\times$ larger. The particular values of λ and ν matter very little as long as they are in the regime of slow immigration. (The opposite regime where immigration is substantial can be qualitatively different because immigration can stabilize the populations of phage and bacteria strains which would otherwise go extinct). Finally, the particular value of the phage burst size b has very little effect on our results since the ecological fixed point depends on $\frac{d}{dn_p}\log b_{n_p}$ (and is therefore unchanged when b is modified by a multiplicative factor; Eq. (S5)) and the qualitative dynamical behavior is mostly determined by α/δ as described in Section S4. Natural phage burst sizes are typically of $\mathcal{O}(100)$ phage particles per burst, but also are accompanied by a sizeable time delay between phage infection and lysis. Given that our model neglects this time delay, the effective burst size must be decreased to reproduce overall phage proliferation rates. $b^{\max} = 15$ was therefore chosen to correspond to a burst size of ~ 200 for a system with a typical lysis time [S2].

We implement concave cost functions $g(n_b) = \alpha^{\max} \cos\left(\frac{\pi n_b}{2n_b^{\max}}\right)$ and $h(n_p) = b^{\max} \cos\left(\frac{\pi n_p}{2n_p^{\max}}\right)$. $n_b^{\max}$ sets the maximum number of defense systems bacteria can have before their growth rate α reaches zero, and is somewhat larger than n_b^{pos} which is determined by the net growth rate $\alpha - \mu$ reaching zero (and similarly for $n_p^{\max}$ for phage). Strains with more systems than the maximum don't grow: $g(n_b \geq n_b^{\max}) = 0$, and similarly, $h(n_p \geq n_p^{\max}) = 0$. In our simulations, we set $n_b^{\max} = 3.27$, and $n_p^{\max} = 4.5$, as these values yielded $(n_b^\star, n_p^\star) = (2, 3)$ and $(n_b^{\text{pos}}, n_p^{\text{pos}}) = (3, 4)$ for our parameter choices.

In all simulations, the growth rates of individual bacterial strains α_i, the burst sizes of individual phage strains b_j, and the infection rates k_{ij} were all varied at order 10^{-5}. Specifically, these terms were multiplied by $\left(1 + 10^{-5} \times (2r - 1)\right)$ where r is a random number uniformly distributed between 0 and 1, chosen randomly and independently for each strain or strain-strain interaction. Thus, small amounts of parameter heterogeneity are added to the system; for example, values of k ultimately range from $(1 - 10^{-5})$ to $(1 + 10^{-5})$.

We ran each simulation for 10^7 time units (equivalent to 1.4×10^6 bacterial generations for $\alpha/\delta = 0.1$, or to more generations for larger α).

We also ran simulations initializing the system with only bacterial strains for which $n_b = n_b^\star$ and phage strains with $n_p = n_p^\star$, and setting the immigration fluxes to zero, $\lambda = \nu = 0$. We found qualitatively and quantitatively similar results to those displayed in Fig. 1b-e, and observed no phage or bacterial strains going extinct over the course of these simulations. The simulations in Fig. 1f-g were performed in this manner.

To measure the Lyapunov exponent, we initialized two trajectories using the parameters of Fig. 1b,c, with initial values of phage populations $\sim 10^{-14}$ higher in one trajectory than the other. Specifically, the initial values in the second simulation were equal to those of the first, plus $10^{-14} \times (2r - 1)$, where r is a uniformly distributed random number between 0 and 1 chosen independently for each phage strain. We then measured the distance between the two trajectories as $\sqrt{(B - B')^2}$ where B is the total bacterial population. This value grows exponentially until ~ 400 generations, at which point it begins fluctuating between 10^{-5} and 10^0. This behavior of the distance between trajectories initialized nearby (namely, exponential growth, followed by fluctuations around a fixed value) is typical of chaotic systems. The Lyapunov exponent is defined as the slope of the exponential growth segment. To measure this, the logarithm of the distance was fit to a line (or equivalently, the distance was fit to an exponential). This analysis was repeated ten times for different instantiations of r, with measurements of the Lyapunov exponent having a mean of 0.0822 and a standard deviation of 0.0014.

In Fig. 1g, we needed to measure the dynamic ratio in a consistent way for both chaotic and oscillatory systems. To do this, first, we identified the local peaks and troughs (i.e. where the derivatives of the population densities change sign). For oscillatory systems, the peaks are all at (very nearly) equal values, as are the troughs. For chaotic systems, this is not the case. In order to measure the peaks and troughs in a manner that does not change much between different instantiations of the chaotic dynamics, we therefore defined the dynamic ratio as the ratio of the 90^{th} percentile of the local population density peaks to the 10^{th} percentile of the local population density troughs. The dynamic timescale was measured by taking the median of the time between local maxima and the median of the time between local minima, and averaging these two medians. For oscillatory systems, this measures the period of oscillations.

The simulations in Fig. 1f-g were initiated at $B_i = 0.06 \times (1 + r)$ and $P_j = 0.06 \times (1 + r)$ where r is a random number uniformly distributed between 0 and 1, chosen independently for each bacterial and each phage strain. Qualitatively similar results were obtained for simulations initiated at $B_i = B^{\text{fp}}_{n_b^\star} \times (1 + r)$ and $P_j = P^{\text{fp}}_{n_p^\star} \times (1 + r)$, i.e. where the initial conditions depend on parameter values through the dynamical fixed-point population densities.

Finally, we developed a variant of these simulations to take into account the stochasticity of evolutionary dynamics. Rather than initiating the system with all strains present, we initialized the system with only one bacterial strain (with one defense system), and one phage strain (with the corresponding counter-defense system). After every 5 timepoints of simulation, we performed a mutation step. In this mutation step, new bacterial or phage strains could be created, by either gaining or losing defense or counter-defense systems. First, we choose whether to mutate the bacteria (with probability p) or the phage (with probability $1 - p$); we chose $p = 10^{-2}$ to approximate the challenge bacteria face in constructing new defense systems as opposed to the relative simplicity of phage counter-defense systems, as discussed in the previous section. Next, we select the strain to mutate, proportionally to its population density at the time of the mutation step. We then determine whether the mutation will be the (a) gain or (b) loss of defense (or counter-defense) systems, each occurring with probability $1/2$. Finally, all possible single mutants either adding or removing a defense or counter-defense system (depending on which was selected) from the selected strain are added to the system at a small initial population (10^{-15}), or if they were already present, their population is increased by the same small amount. These simulations resulted in the same qualitative behavior as the constant immigration rate simulations

discussed in the main text, evolving towards the ecologically stable fixed point at the system level, and exhibiting chaotic dynamics at the population level.

S4 Dynamical analysis

To understand the dynamical behavior of the system, we turn to the $n^{\text{tot}} = 0$ case, which we refer to as the 1:1 case since it involves a single bacterial strain and a single phage strain. In Fig. 1f-g, we show that certain aspects of the dynamical behavior of the 1:1 case closely parallel those of systems with $n^{\text{tot}} > 0$. In this section, we quantitatively analyze the 1:1 case.

First, we perform linear stability analysis to describe the behavior of the system near the dynamical fixed point (Eqs. (S1)). The essential element of linear stability analysis is the calculation of the eigenvalues of the Jacobian matrix at the dynamical fixed point. For the 1:1 case, the eigenvalues are $\pm i\sqrt{\delta\,(\alpha-\mu)}$. That these are imaginary indicates that the 1:1 case undergoes continued oscillations. The period of these oscillations is given by $2\pi/\sqrt{\delta\,(\alpha-\mu)}$. This prediction is plotted as a dashed gray curve in the inset to Fig. 1g.

Predicting the amplitude of oscillations is less straightforward, and to our knowledge no generic method enables this prediction. Linear stability analysis provides no information regarding the amplitude of oscillations. To address this challenge, we recognize that there is a quantity C satisfying $dC/dt = 0$. In general, this quantity is given by

$$C = P^{\text{fp}}_{n_p} \sum_j \left(\frac{P_j(t)}{P^{\text{fp}}_{n_p}} - \log \frac{P_j(t)}{P^{\text{fp}}_{n_p}} \right) + bB^{\text{fp}}_{n_b} \sum_i \left(\frac{B_i(t)}{B^{\text{fp}}_{n_b}} - \log \frac{B_i(t)}{B^{\text{fp}}_{n_b}} \right). \tag{S6}$$

For the 1:1 case, this quantity simplifies to

$$C = P^{\text{fp}}_0 \left(\frac{P(t)}{P^{\text{fp}}_0} - \log \frac{P(t)}{P^{\text{fp}}_0} \right) + bB^{\text{fp}}_0 \left(\frac{B(t)}{B^{\text{fp}}_0} - \log \frac{B(t)}{B^{\text{fp}}_0} \right), \tag{S7}$$

where P^{fp}_0 and B^{fp}_0 are given by Eqs. (S1) with $n_p = n_b = n^{\text{tot}} = 0$.

Because C is a constant in time, it will also be a constant when P or B are at an extremum. Solving for B at either extremum of P (i.e. where $dP/dt = 0$) yields $B = B^{\text{fp}}_0$. Similarly, solving for P at either extremum of B yields $P = P^{\text{fp}}_0$. Thus, we find that

$$\begin{aligned} C &= P^{\text{ext}} - P^{\text{fp}}_0 \log \frac{P^{\text{ext}}}{P^{\text{fp}}_0} + bB^{\text{fp}}_0 \\ &= bB^{\text{ext}} - bB^{\text{fp}}_0 \log \frac{B^{\text{ext}}}{B^{\text{fp}}_0} + P^{\text{fp}}_0, \end{aligned} \tag{S8}$$

where B^{ext} represents the value of $B(t)$ at its maximum or minimum, and similarly for P^{ext}.

We then estimate the values of P^{min}, P^{max}, B^{min}, and B^{max}. For the minimum values, we treat the linear terms (e.g. P^{ext}) as negligible compared to the logarithmic terms; for the maximum values, we treat the logarthmic terms as negligible. These approximations yield

$$\begin{aligned} C &= P^{\text{max}} + bB^{\text{fp}}_0, \\ &= -P^{\text{fp}}_0 \log \frac{P^{\text{min}}}{P^{\text{fp}}_0} + bB^{\text{fp}}_0, \\ &= bB^{\text{max}} + P^{\text{fp}}_0, \\ &= -bB^{\text{fp}}_0 \log \frac{B^{\text{min}}}{B^{\text{fp}}_0} + P^{\text{fp}}_0. \end{aligned} \tag{S9}$$

Solving for the extrema and simplifying, we find that the dynamic ratios of B and of P are given by:

$$\begin{aligned}\frac{B^{\max}}{B^{\min}} =& \frac{C - P_0^{\text{fp}}}{bB_0^{\text{fp}}} \exp\left[\frac{C - P_0^{\text{fp}}}{bB_0^{\text{fp}}}\right], \\ \frac{P^{\max}}{P^{\min}} =& \frac{C - bB_0^{\text{fp}}}{P_0^{\text{fp}}} \exp\left[\frac{C - bB_0^{\text{fp}}}{P_0^{\text{fp}}}\right].\end{aligned} \tag{S10}$$

To understand the growth of the dynamic ratio of B for large α/δ and of P for small α/δ, we first recognize that the positivity of the dynamic ratios implies $C > P_0^{\text{fp}}$ and $C > bB_0^{\text{fp}}$, so that the dynamic ratios can be approximated as

$$\begin{aligned}\frac{B^{\max}}{B^{\min}} \approx& \frac{C}{bB_0^{\text{fp}}} \exp\left[\frac{C}{bB_0^{\text{fp}}}\right], \\ \frac{P^{\max}}{P^{\min}} \approx& \frac{C}{P_0^{\text{fp}}} \exp\left[\frac{C}{P_0^{\text{fp}}}\right].\end{aligned} \tag{S11}$$

Substituting in from Eqs. (S9), we find

$$\begin{aligned}\frac{B^{\max}}{B^{\min}} \approx& \frac{bB^{\max} + P_0^{\text{fp}}}{bB_0^{\text{fp}}} \exp\left[\frac{bB^{\max} + P_0^{\text{fp}}}{bB_0^{\text{fp}}}\right], \\ \frac{P^{\max}}{P^{\min}} \approx& \frac{P^{\max} + bB_0^{\text{fp}}}{P_0^{\text{fp}}} \exp\left[\frac{P^{\max} + bB_0^{\text{fp}}}{P_0^{\text{fp}}}\right].\end{aligned} \tag{S12}$$

Finally, substituting in for the dynamical fixed point values (Eqs. (S1)), we arrive at

$$\begin{aligned}\frac{B^{\max}}{B^{\min}} \approx& \left(\frac{B^{\max}}{B_0^{\text{fp}}} + \frac{\alpha - \mu}{\delta}\right) \exp\left[\left(\frac{B^{\max}}{B_0^{\text{fp}}} + \frac{\alpha - \mu}{\delta}\right)\right], \\ \frac{P^{\max}}{P^{\min}} \approx& \left(\frac{P^{\max}}{P_0^{\text{fp}}} + \frac{\delta}{\alpha - \mu}\right) \exp\left[\left(\frac{P^{\max}}{P_0^{\text{fp}}} + \frac{\delta}{\alpha - \mu}\right)\right].\end{aligned} \tag{S13}$$

For large α (i.e. $\alpha \gg \delta$), the dynamic ratio of B is therefore dominated by $e^{\alpha/\delta}$. Similarly, for small α (i.e. $\alpha - \mu \ll \delta$), the dynamic ratio of P is dominated by $e^{\delta/(\alpha-\mu)}$.

To find the crossover between the two dynamic regimes (one where the dynamic ratio of B is large, and the other where the dynamic ratio of P is large), we solve for

$$\frac{B^{\max}/B^{\min}}{P^{\max}/P^{\min}} = 1 \qquad \text{(at crossover)}. \tag{S14}$$

Starting from Eq. (S11), this can be approximated as

$$\frac{P_0^{\text{fp}}}{bB_0^{\text{fp}}} \approx \exp\left[C\left(\frac{1}{bB_0^{\text{fp}}} - \frac{1}{P_0^{\text{fp}}}\right)\right] \qquad \text{(at crossover)}. \tag{S15}$$

While the precise value of C depends on the particular initial conditions chosen, it can be estimated by its value at the fixed point, $C^{\text{fp}} = P_0^{\text{fp}} + bB_0^{\text{fp}}$. This yields

$$\frac{P_0^{\text{fp}}}{bB_0^{\text{fp}}} \approx \exp\left[\frac{P_0^{\text{fp}}}{bB_0^{\text{fp}}} - \frac{bB_0^{\text{fp}}}{P_0^{\text{fp}}}\right] \qquad \text{(at crossover)}. \tag{S16}$$

The equation $x = \exp\left[x - x^{-1}\right]$ is solved by $x = 1$. Therefore, the crossover occurs at

$$P_0^{\text{fp}} \approx bB_0^{\text{fp}} \qquad \text{(at crossover)}, \tag{S17}$$

or, substituting in for the dynamical fixed point values (Eqs. (S1)),

$$\alpha - \mu \approx \delta \qquad \text{(at crossover)}. \tag{S18}$$

Supplemental References

[S1] Sarah Camara-Wilpert, David Mayo-Muñoz, Jakob Russel, Robert D. Fagerlund, Jonas S. Madsen, Peter C. Fineran, Søren J. Sørensen, and Rafael Pinilla-Redondo. Bacteriophages suppress CRISPR–Cas immunity using RNA-based anti-CRISPRs. Nature, 623(7987):601–607, 2023.

[S2] Ofer Kimchi, Yigal Meir, and Ned S Wingreen. Lytic and temperate phage naturally coexist in a dynamic population model. The ISME Journal, 18(May):1–5, 2024.